Mon. Not. R. Astron. Soc. **000**, 1–?? (2012) Printed 24 June 2015 (MN LATEX style file v2.2)

# On the dependence of the X-ray continuum variations with luminosity in accreting X-ray pulsars

K. A. Postnov[1,4], M. I. Gornostaev[1,4], D. Klochkov[2], E. Laplace[2], V. V. Lukin[3], N. I. Shakura[4] ⋆

[1] *Faculty of Physics, M. V. Lomonosov Moscow State University, Leninskie Gory, Moscow 119991 Russia*
[2] *Institute of Astronomy and Astrophysics, Karl-Eberhard University, Tübingen, Sand 1, D-72076, Germany*
[3] *M.V. Keldysh Institute of Applied Mathematics RAS, Miusskaya sq., 4, Moscow, Russia*
[4] *Sternberg Astronomical Institute, Moscow M.V. Lomonosov State University, Universitetskij pr., 13, 119992, Moscow, Russia*



Received ... Accepted ...

**ABSTRACT**

Using RXTE/ASM archival data, we investigate the behaviour of the spectral hardness ratio as a function of X-ray luminosity in a sample of six transient X-ray pulsars (EXO 2030+375, GX 304-1, 4U 0115+63, V 0332+63, A 0535+26 and MXB 0656-072). In all sources we find that the spectral hardness ratio defined as $F_{5-12\mathrm{keV}}/F_{1.33-3\mathrm{keV}}$ increases with the ASM flux (1.33–12 keV) at low luminosities and then saturates or even slightly decreases above some critical X-ray luminosity falling into the range $\sim (3-7)\times 10^{37}$ erg s$^{-1}$. Two-dimensional structure of accretion columns in the radiation-diffusion limit is calculated for two possible geometries (filled and hollow cylinder) for mass accretion rates $\dot{M}$ ranging from $10^{17}$ to $1.2\times10^{18}$ g s$^{-1}$. The observed spectral behaviour in the transient X-ray pulsars with increasing $\dot{M}$ can be reproduced by a Compton saturated sidewall emission from optically thick magnetized accretion columns with taking into account the emission reflected from the neutron star atmosphere. At $\dot{M}$ above some critical value $\dot{M}_{cr} \sim (6-8)\times 10^{17}$ g s$^{-1}$, the hight of the column becomes such that the contribution of the reflected component to the total emission starts decreasing, which leads to the saturation and even slight decrease of the spectral hardness. Hollow-cylinder columns have a smaller height than the filled-cylinder ones, and the contribution of the reflected component in the total emission does not virtually change with $\dot{M}$ (and hence the hardness of the continuum monotonically increases) up to higher mass accretion rates than $\dot{M}_{cr}$ for the filled columns.

**Key words:** accretion - pulsars:general - X-rays:binaries

## 1 INTRODUCTION

Accretion of matter onto a gravitating centre is a ubiquitous physical process in astrophysics. The matter gravitationally captured from the surrounding rarefied medium by a body of mass $M$ (or, if in a binary system, escaping from the secondary star as a stellar wind or due to Roche lobe overflow) eventually reaches the surface of the body with the velocity of the order of the parabolic one, $v = \sqrt{2GM/R}$, where $R$ is the radius of the body. This velocity becomes very high in the case of accretion onto a compact star. For neutron stars with radius $R_{NS} \sim 10$ km the velocity reaches $\sim 10^{10}$ cm s$^{-1}$, so that the accretion energy release is $L \sim 0.1\dot{M}c^2$, where $\dot{M}$ is the mass accretion rate and $c$ is the velocity of light. These basic facts required the calculation of the accreting matter braking near the compact star surface. In the pioneer work by Zel'dovich & Shakura (1969), the structure of the shock wave produced by spherically symmetric accreting matter near the neutron star surface without magnetic field was calculated. Braking of the accreting matter was assumed to be primarily due to Coulomb interactions of the infalling protons with the surface, which is justified at low accretion rates when interaction of the charged particles with radiation is insignificant.

Immediately after the discovery of X-ray pulsars in 1971 (Giacconi et al. 1971) it was realized that in bright pulsars the radiation plays a crucial role in braking of the accreting matter onto the surface of a neutron star with strong magnetic field. Indeed, in this case the matter is canalized by the neutron star magnetic field onto the magnetic polar caps, which are characterized by a small radius $r_0 \approx R_{NS}\sqrt{R_{NS}/R_A} \sim 10^5$ cm (for a purely dipole field), where $R_A$ is the magnetosphere radius.

It is now well recognized that once the radiation density above the polar cap starts playing the role in the accreting matter dynamics, an optically thick accretion column above the polar cap is formed (Basko & Sunyaev 1976) (see Mushtukov et al. (2015) for the latest investigation). The characteristic height of the column increases with accretion rate, most of the emission escapes through

⋆ E-mail: pk@sai.msu.ru

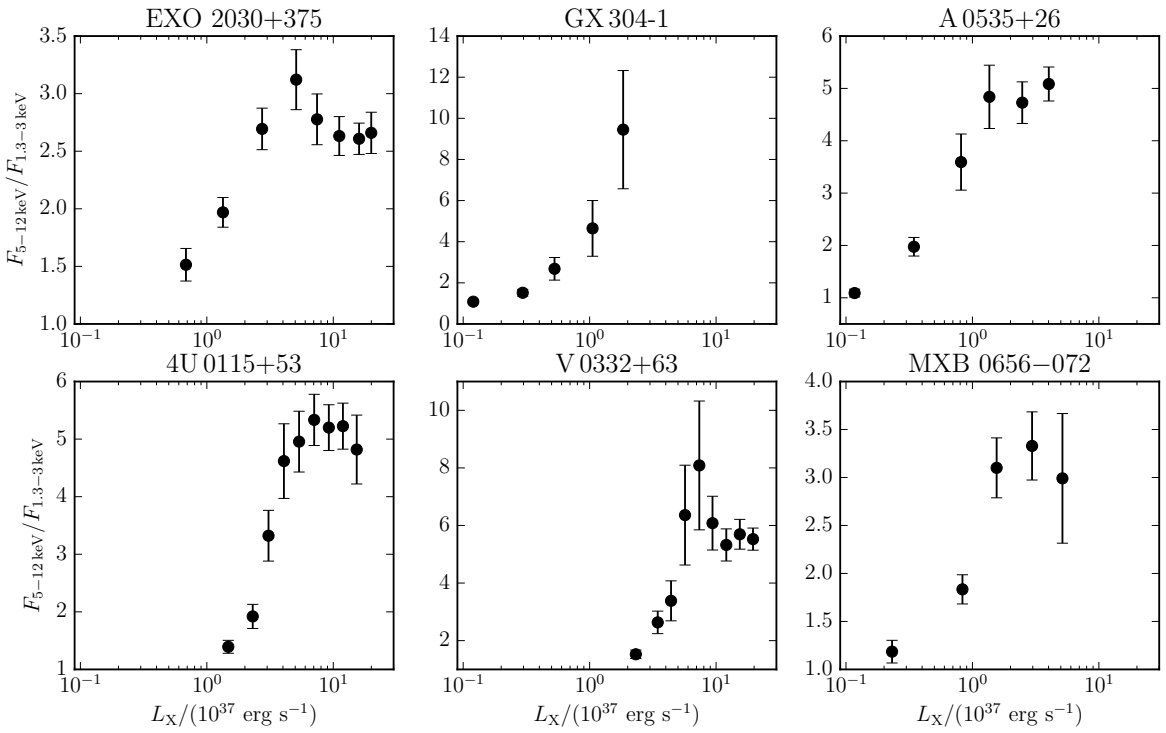


**Figure 1.** The ratio of the fluxes in 5–12 keV and 1.33–3 keV ranges (referred to as "hardness ratio" in text) measured with RXTE/ASM for six transient accreting pulsars as a function of the total ASM flux in the 1.33–12 keV range.

sidewalls, and it can be expected that above some X-ray luminosity the dependence of the observed properties of the continuum emission on the X-ray luminosity can become different from that in the low-luminosity regime.

Here we stress that the effects of the strong magnetic field are important for the observed properties of X-ray continuum at energies below the cyclotron line energy due to scattering processes which have different cross-sections for different photon polarization modes. At small accretion rates, the accretion mound can be viewed as a thin slab, and mostly ordinary photons (for which the electron scattering cross-section is strongly angular dependent but frequency independent) escape along the magnetic field lines forming a pencil-beam X-ray emission diagram (Basko & Sunyaev 1975). In contrast, when the accretion column is formed at higher X-ray luminosities, mostly extraordinary photons (for which the electron scattering cross-section is angle independent but strongly frequency dependent) escape sidewall to form a fan-like X-ray emission beam (Lyubarskii 1986).

Presently, there is a wealth of observational data on X-ray pulsars that can be used to check different regimes of accretion onto magnetized neutron stars. Different types of spectrum–luminosity dependence were first discovered based on the behavior of cyclotron resonant scattering features (CRSFs) (e.g. Tsygankov et al. (2006); Staubert et al. (2007); Klochkov et al. (2011); Becker et al. (2012); Nishimura (2014)).

However, the mechanism of the CRSF generation in accretion columns of accreting neutron stars is still not well understood due to a very complicated physics of radiation transfer in superstrong magnetic fields of neutron stars. For example, recently a novel model for CRSF production in spectra of bright X-ray pulsars due to reflection of the radiation generated in the accretion column from the neutron star surface was proposed (Poutanen et al. 2013). This model can successively explain the CRSF energy dependence on luminosity observed in outbursts of the transient X-ray pulsar V 0332+53 (see also (Lutovinov et al. 2015) for further applications of the model). From the observational point of view, the study of CRSFs is a challenging task because it requires long dedicated observations using the instruments with high effective area and spectral resolution above 20–30 keV. Only in a fraction of accreting pulsars CRSFs are reliably measured (Caballero & Wilms 2012; Revnivtsev & Mereghetti 2014).

Recently, Klochkov et al. (2011) and Reig & Nespoli (2013) pointed out that in addition to the CRSF behaviour, different types of the spectrum–luminosity dependence in accreting pulsars can be probed by studying the variability of the X-ray continuum with luminosity. Specifically, it was found that the X-ray continuum described by a power-law dependence $F_\mathrm{X} \sim E^\Gamma$ becomes *harder* with increasing X-ray flux in X-ray pulsars showing a *positive* correlation of the CRSF energy $E_c$ with flux, whereas it becomes *softer* or virtually does not change with increasing flux in pulsars showing a negative $E_c(F_\mathrm{X})$-correlation (Figs. 3 and 6 in Klochkov et al. (2011)). Clearly, the continuum studies are much less demanding from the point of view of data analysis than the spectroscopic analysis of the CRSF behaviour (if the CRSF is reliably identified in the X-ray pulsar spectrum at all).

The purpose of the present paper is to perform model 2D calculations of the accretion column structure in the radiation diffusion approximation and to calculate the emerging X-ray continuum in order to see how the hardness of the sidewall emission from accretion columns with different geometries (a filled or hollow cylinder) changes with accretion rate variations in the regime of radiation-dominated accretion flow braking. We calculate the sidewall energy flux escaping from the optically thick accretion column and the saturated Compton spectrum of extraordinary photons. We find

that for typical parameters of X-ray pulsars (the neutron star surface magnetic field $B = 3 \times 10^{12}$ G, mass accretion rate onto one pole $\dot{M} = (1-12)\times 10^{17}$ g s$^{-1}$), with increasing mass accretion rate the hardness of the emergent sidewall emission from the column always increases. The sidewall emission from the column is Doppler-boosted by unbraked matter in the external part of the column toward the neutron star surface. The reflected radiation from the neutron star atmosphere calculated in the single-scattering approximation is harder than the incident emission, and its addition to the total flux form the column renders the spectrum even harder. However, starting from some accretion rate the height of the column increases such that the fraction of the reflected radiation in the total flux starts decreasing. This purely geometrical effect leads to the saturation of the hardness ratio at $\dot{M}_{cr} \sim (6-8) \times 10^{17}$ g s$^{-1}$ (for the assumed neutron star parameters). In the case of the hollow-cylinder accretion column geometry, the saturation of the spectral hardness has not been reached in the calculated range of mass accretion rates due to smaller photon diffusion times across the columns thickness and correspondingly smaller heights of such columns, when the contribution of the emission reflected from the neutron star surface always dominates.

The structure of the paper is as follows. In Section 2 we briefly describe the observed correlations of CRSF with X-ray flux and X-ray continuum properties with X-ray flux. In Section 3 the basic equations of the structure of the radiation-supported columns and their numerical solution are described. The results of calculations of the spectrum are presented in Section 4, which is followed by the summary and conclusions.

## 2 OBSERVATIONS

There is a growing number of X-ray pulsars showing the dependence of $E_c$ of their X-ray flux (e.g., Becker et al. (2012) and references therein). The cyclotron energy $E_c$ in the bright transient X-ray pulsar V 0332+53 decreases with luminosity $L_X$ (Tsygankov et al. 2006; Tsygankov, Lutovinov & Serber 2010). A similar negative $E_c(L_X)$-correlation has been reported for another bright transient pulsar 4U 0115+63 (Tsygankov et al. 2007; Mihara, Makishima & Nagase 2004). Recently, however, this correlation has been questioned by Müller et al. (2013), who argued that the $E_c(L_X)$-correlation in 4U 0115+63 is an artefact related to the continuum modelling (see also Boldin, Tsygankov & Lutovinov (2013) for an independent analysis).

There is another type of X-ray pulsars with lower X-ray luminosities and somewhat higher magnetic fields which exhibit a *positive* correlation of $E_c$ with $L_X$: Her X-1 (Staubert et al. 2007), GX 304−1 (Yamamoto et al. 2011; Klochkov et al. 2012), and probably Vela X−1 (Fürst et al. 2014) and A 0535+26 (Klochkov et al. 2011; Müller et al. 2013).

As mentioned in the Introduction, a similar bimodality is observed in the dependence of the X-ray continuum hardness on luminosity. This dependence can be studied using, for example, data from all-sky monitors such as RXTE/ASM and MAXI, i.e. without dedicated spectroscopic observations which are necessary to measure CRSFs. Following this approach, we measured the hardness ratio as a function of luminosity in the accreting pulsars GX 304−1, 4U 0115+63, V 0332+53, EXO 2030+375, A 0535+26 and MXB 0656072 using the data from different energy bands of RXTE/ASM. The result is shown in Fig. 1. To convert the ASM count rates into X-ray luminosities, we used published distances to the sources (GX 304−1: ∼2 kpc, Parkes, Murdin & Mason 1980; 4U 0115+63: ∼7 kpc, Negueruela & Okazaki 2001, V 0332+53: ∼7 kpc, Negueruela et al. 1999; EXO 2030+375: ∼7 kpc, Wilson et al. 2002; A 0535+26: ∼ 2 kpc, Steele et al. 1998; MXB 0656-072: ∼ 3.9 kpc, McBride et al. 2006) and their broadband X-ray spectra from the archival pointed observations with INTEGRAL and RXTE available to us. One can see that at lower fluxes the hardness ratio increases with flux. At a certain flux, however, a flattening of the hardness ratio is observed in 4U 0115+63, V 0332+53, EXO 2030+375, A 0535+26 and MXB 0656072. This 'turnover' occurs at the flux roughly corresponding luminosities $(3-7) \times 10^{37}$ erg s$^{-1}$. In GX 304−1, which does not show such a turnover, this 'critical' luminosity has simply not been reached during the outbursts registered by RXTE ASM.

A similar dependence of spectral properties on the X-ray flux at luminosities below $\sim 10^{37}$ erg s$^{-1}$ was also reported from spectroscopic observations of the transient Be-X-ray pulsar GRO J1008-57 Kühnel et al. (2014).

At the lowest energies covered by RXTE/ASM, the spectrum of accreting pulsars is significantly affected by photo-electric absorption caused mostly by matter in the vicinity of the source. Such an absorption naturally influences the derived hardness ratios and cannot be accounted for without a high-resolution spectral analysis using pointed observations. Neutral absorbing matter surrounding the accretor might correlate with the mass transfer rate in the binary and might therefore be proportional to the X-ray luminosity of the pulsar. Such an effect might at least contribute to the observed positive correlation between the hardness ratio and flux. However, we do not expect any break in the slope of the correlation between the absorption column density and flux at $L_X \sim 10^{37}$ erg s$^{-1}$ (although we cannot exclude this possibility). We therefore identify the observed breaks with those reported by Reig & Nespoli (2013) at similar X-ray luminosities based on the data from RXTE/PCA observations taken at higher energies which should be unaffected by the photo-electric absorption.

## 3 ACCRETION COLUMN STRUCTURE IN THE RADIATION DIFFUSION LIMIT

### 3.1 Qualitative considerations

At high luminosities, $L_X \gtrsim 10^{37}$ erg s$^{-1}$, the radiation pressure dominates, and the braking of the accreting matter flow is due to interaction with photons. In this case, the kinetic energy of falling particles $m_p v_0^2/2$, where $v_0 = 10^{10}$ cm s$^{-1}$ is the free-fall velocity near the NS surface, decreases by almost 99% at optical depths $\tau \sim (2-3)(c/v_0) \sim 4-9$. This was shown for the first time by Davidson (1973), and in a wide range of parameters was calculated by Wang & Frank (1981) by solving two-dimensional gas-dynamic equations with diffusive radiation transfer. As a result, the shape of the zone of energy release looks like a 'mound' with the characteristic height $z_0 \sim r_0$.

With further increasing X-ray luminosity above $L_X > L^*$, as was first shown by Basko & Sunyaev (1976), the height of the braking zone starts increasing, and instead of a 'mound' an optically thick accretion column appears with $z_0 > r_0$. Most of the kinetic energy of the accreting flow is transformed into heat at around $z_0$ (which sometimes is referred to as the height of the radiation-dominated shock), and below this height the matter settles down towards the column base. The thermal energy is advected by the settling matter with an effective velocity of $v \sim 0.1 v_0$, and the generated heat finally escapes through the column sidewalls.

It is possible to estimate the critical luminosity $L^*$ by equating the dynamical time of the fall of matter to the diffusion time of photons across the column. The characteristic settling time is clearly $t_s = z_0/v$. The characteristic time of the radiation diffusion across the filled cylinder column is

$$t_d \simeq \frac{r_0^2}{\nu_d} \simeq \frac{r_0^2 \varkappa_\perp}{c}\rho = \frac{r_0^2 \varkappa_\perp}{c}\frac{S}{v} \quad (1)$$

where we have eliminated the density $\rho$ using the mass continuity equation

$$S = \rho v = \frac{\dot{M}}{\pi r_0^2}\,. \quad (2)$$

In the case of a hollow cylinder with wall thickness $br_0$ the diffusion time decreases with $b$:

$$t_d \simeq \frac{b^2 r_0^2}{\nu_d} \simeq \frac{b^2 r_0^2 \varkappa_\perp}{c}\rho = \frac{b^2 r_0^2 \varkappa_\perp}{c}\frac{S}{v} = \frac{b\varkappa_\perp}{c}\frac{\dot{M}}{\pi v} \quad (3)$$

By equating $t_s = t_d$ and noting that the velocity is crossed out, we arrive at the expression

$$z_{0,f} = \frac{\varkappa_\perp}{\pi c}\dot{M}\,, \quad z_{0,h} = \frac{b\varkappa_\perp}{\pi c}\dot{M} \quad (4)$$

for the filled and hollow cylinder geometries, respectively.

Now, by equating $z_0 = r_0$, we find the critical mass accretion rate $\dot{M}^*$ and the corresponding X-ray luminosity

$$L^* = 0.1\dot{M}^* c^2 = \frac{\pi c}{b\varkappa_\perp} 0.1 c^2 r_0 \approx 2.36{\times}10^{36}[\mathrm{erg\ s^{-1}}]\left(\frac{r_0}{10^5\mathrm{cm}}\right)\left(\frac{b\varkappa_\perp}{\varkappa_T}\right)^{-1}. \quad (5)$$

Here the factor $b$ should be set one for the filled cylinder geometry.

It is important to realize that the accurate value of $L^*$ should be found from two-dimensional numerical calculations of the radiation transfer equations, and, for example, Wang & Frank (1981) found

$$L^* \approx 5.25\times10^{36}[\mathrm{erg\ s^{-1}}]\left(\frac{E_c}{\bar{E}}\right)^{2/5}\left(\frac{r_0}{10^5\mathrm{cm}}\right)\left(\frac{M}{1.5M_\odot}\right) \quad (6)$$

Here the factor $(E_c/\bar{E})$ takes into account the effective change in the photon scattering cross-section in the strong magnetic field and the deviation of the magnetic field line geometry from the simple cylindrical case near the NS surface. This factor is $\sim 1$ if the mean photon energy $\bar{E} > E_c$. It is seen that our simple estimate Eq. (5) derived above is consistent with this value to within a factor of two. Recently, the critical luminosity was reassessed by Mushtukov et al. (2015) who found it to vary by almost an order of magnitude (depending on the magnetic field) within an interval centred at $\sim 10^{37}$ erg s$^{-1}$.

Therefore, the qualitative considerations presented above suggest the increase in the accretion structure height $z_0 \propto \dot{M}$ above some critical luminosity $\sim 10^{37}$ erg s$^{-1}$ (see also a more detailed derivation in Arons (1992), Section 3.).

### 3.2 Numerical simulations of axially symmetric accretion column

Qualitative considerations described above can be made more precise by numerical calculations of steady-state accretion columns. This radiation-hydrodynamic problem, complicated by the need to calculate the radiation transfer in a strong magnetic field, has not been solved self-consistently as yet. However, the structure of an optically thick accretion column at luminosities above $10^{37}$ erg s$^{-1}$ can be calculated in the radiation diffusion approximation with grey scattering coefficients along and perpendicular to the magnetic field lines (Davidson 1973; Basko & Sunyaev 1976; Wang & Frank 1981). The emergent radiation spectrum will be formed due to scattering of photons on electrons in the optically thin outer layers, which is a separate problem (see the next Section).

We shall consider two possible axially symmetric geometries of accretion columns: a filled cylinder of radius $r_0$ and a hollow cylinder of the inner radius $r_0$ and thickness $br_0$. In both cases $r_0$ is determined by the magnetosphere radius $R_A$, and in the second case the wall thickness $br_0$ can be related to the distance the disc matter enters the magnetosphere before being completely frozen into the magnetic field. We shall assume a purely dipole magnetic field and the disc matter frozen at a fixed fraction of the Alfvén radius.

From the definition of the Alfvén radius, $R_A \propto \dot{M}^{-\frac{2}{7}}$, and the expression for the polar cap radius $r_0$ we see that the polar cap radius scales with accretion rate as $r_0 \propto \dot{M}^{\frac{1}{7}}$. The freezing depth of disc plasma at the Alfvén radius is fixed as $\Delta = 0.1R_A$, and since $\frac{\Delta}{R_A} = b$ we have $b \simeq 0.1$. This means that with changing mass accretion rate the thickness of the accretion wall in the case of hollow cylinder geometry changes as $br_0 \propto \dot{M}^{\frac{1}{7}}$ [1].

Note that the value of $b$ is difficult to calculate precisely; it is clear that it should depend on many factors, including the NS magnetic field axis misalignment, the details of the matter entering the magnetosphere due to various instabilities, etc., which are beyond the scope of the present study. However, we should note that in the case of thin cylinder wall, $b \ll 1$, the radiation diffusion time Eq. (1) is proportional $t_d \propto b$, thus decreasing the height of the column $z_0$ at a given mass accretion rate $\dot{M}$. This effect is confirmed by our calculations (see below). The neutron star magnetic field is assumed to be homogeneous across the column. This approximation is justified for not very high accretion heights (especially in the case of the hollow cylinder geometry).

#### 3.2.1 *Boundary conditions*

We are working in cylindrical coordinates $r, \varphi, z$ centred at the columns axis and $z = 0$ at the neutron star surface. The initial velocity of the falling matter at high altitude above the surface of the neutron star is $v_0 = 10^{10}$ cm s$^{-1}$. At the cylinder base ($z = 0$), the velocity is $v = 0$. As a boundary condition at the column side surface we used the relation between the radial energy flux to the energy density $U$ in the form $F_r(r_0, z) = 2cU(r_0, z)/3$, which roughly corresponds to the conditions expected in the scattering atmospheres in the Eddington approximation.

#### 3.2.2 *Basic equations*

The cylindrical symmetry of the problem makes it essentially two-dimensional. The steady-state momentum equation (ignoring gravity, which is very good approximation as discussed e. g. in Basko & Sunyaev (1976)) for accretion braking by the radiation with energy density $U$ reads

$$(\mathbf{S}\cdot\nabla)\,\mathbf{v} = -\frac{1}{3}\nabla U, \quad (7)$$

where $\boldsymbol{S} = \rho\mathbf{v} = \mathrm{const}$ is the mass continuity equation. The integration of these equation yields

[1] In principle, one may consider further complications, e.g., using a specific model of the magnetosphere-disc coupling, like it was done in Mushtukov et al. (2015). This only slightly changes the dependence of $br_0$ on $\dot{M}$.

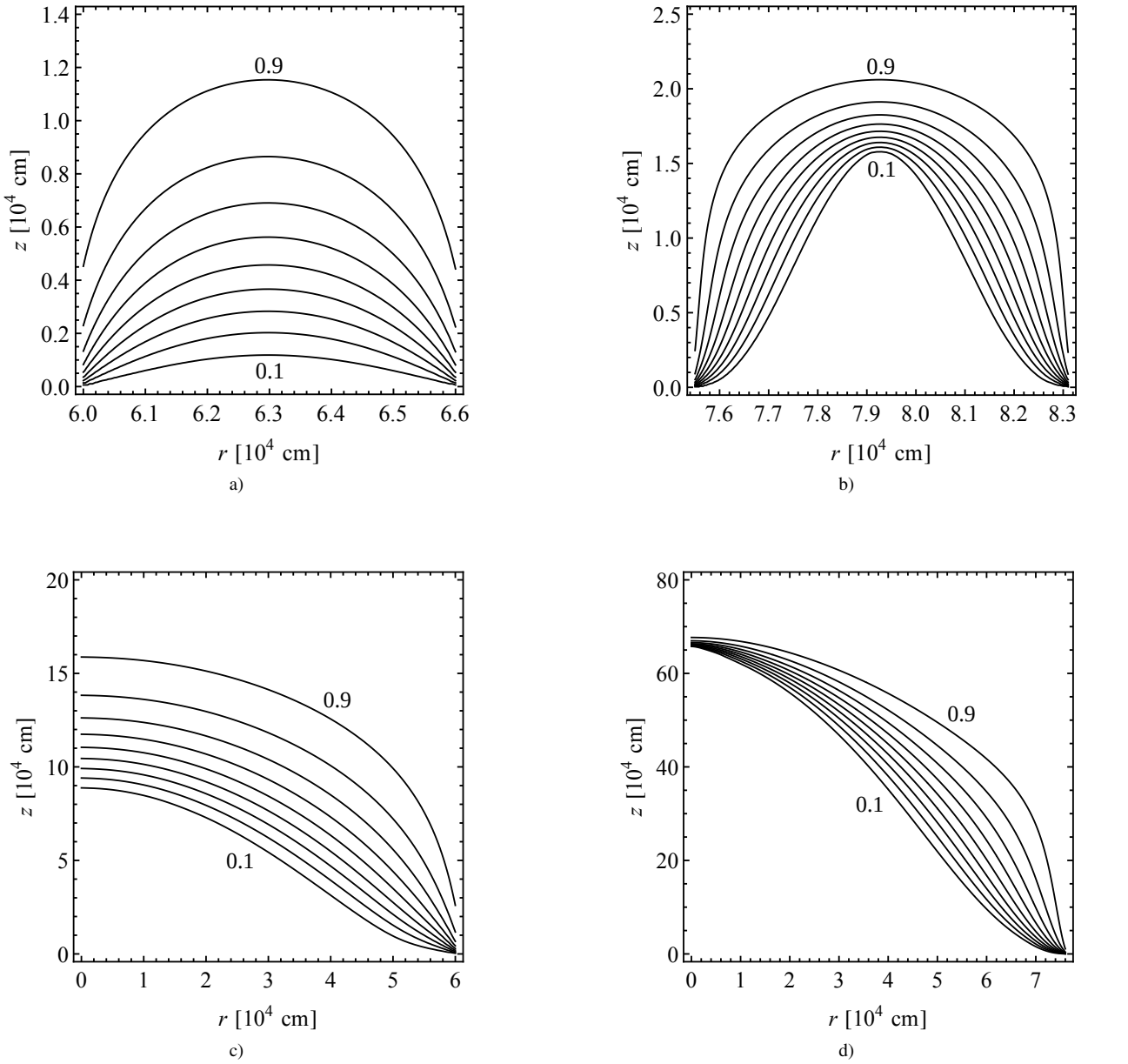


**Figure 2.** Contours of constant $Q$ (0.9 to 0.1, from top to bottom). Top panels: the hollow cylinder geometry with $b = 0.1$ calculated for $\dot{M}_{17} = 1$ (a) and $\dot{M}_{17} = 5$ (b). Bottom panels: the filled cylinder geometry for $\dot{M}_{17} = 1$ (c) and $\dot{M}_{17} = 5$ (d).

$$U = 3S(v_0 - v). \tag{8}$$

Following Davidson (1973), the energy equation can be written as

$$\nabla \cdot \mathbf{F} = -\mathbf{S} \cdot \nabla \left( \frac{v^2}{2} \right), \tag{9}$$

where we has neglected the flow of internal energy of the falling matter.

The radiative transfer equation in the diffusion approximation is

$$\mathbf{F} = -\frac{c}{3\varkappa\rho} \nabla U + \frac{4}{3} U \mathbf{v}, \tag{10}$$

where the inflow of gas is considered to be stationary.

From equation (10) in cylindrical coordinates we find the components of the radiation energy flux:

$$F_r = \frac{-\frac{c}{3\varkappa_\perp \rho} \frac{\partial U}{\partial r}}{1 + \frac{1}{3\varkappa_\perp \rho} \frac{1}{U} \left| \frac{\partial U}{\partial r} \right|}, \tag{11}$$

$$F_z = \frac{-\frac{c}{3\varkappa_\parallel \rho} \frac{\partial U}{\partial z} - \frac{4}{3} U v}{1 + \frac{1}{3\varkappa_\parallel \rho} \frac{1}{U} \left| \frac{\partial U}{\partial z} \right|}. \tag{12}$$

where the coefficients $\left(1 + \frac{1}{3\varkappa_\perp \rho} \frac{1}{U} \left| \frac{\partial U}{\partial r} \right| \right)^{-1}$ and $\left(1 + \frac{1}{3\varkappa_\parallel \rho} \frac{1}{U} \left| \frac{\partial U}{\partial z} \right| \right)^{-1}$ are introduced to use the modified diffusion approximation in the optically thin regions where the change of the radiation energy density on the photon mean free path becomes significant (see Wang & Frank (1981)). Equations (7) – (12) describe the accretion

shock mediated by radiation in the diffusion limit and provide the structure of the zone where most of the accretion energy responsible for the formation of the emergent spectrum is released. The 'sinking zone' downstream the radiation shock, where the matter settles down subsonically and advects thermal energy towards the NS surface, should be treated separately (see e.g. Basko & Sunyaev (1976)). Different physical effects can appear in this zone, e.g. 'photon bubble oscillations' discussed in Arons (1992); Klein et al. (1996).

#### 3.2.3 *Equations in dimensionless form*

The convenient variables are dimensionless velocity of matter squared $Q = v^2/v_0^2$, the dimensionless column radius $\tilde{r} = \varkappa_T S_0 r/c = \tau_T v r/c$ and height $\tilde{z} = \varkappa_T S_0 z/c = \tau_T v z/c$, where $S_0 = S(\dot{M}_{17} = 1) = 8.79 \times 10^6$ erg s$^{-1}$ cm$^{-2}$ (here and below $\dot{M}_{17} = \dot{M}/(10^{17}\,\mathrm{g\,s^{-1}})$ is dimensionless mass accretion rate onto one pole). For the assumed value of $r_0(\dot{M}_{17} = 1)$ the dimensionless factors almost exactly equal to $10^{-4}$ cm$^{-1}$. For the scattering cross-sections we shall assume $\varkappa_\perp = \varkappa_T$ and $\varkappa_T/\varkappa_\parallel = 10$.

With this notation and dimensionless variables, the system of equations (8), (9), (11), (12) is equivalent to one non-linear partial differential equation (cf. Davidson (1973))

$$\tilde{K}_\perp \left[\frac{\partial^2 Q}{\partial \tilde{r}^2} + \frac{1}{\tilde{r}}\frac{\partial Q}{\partial \tilde{r}}\right] + \tilde{K}_\parallel \left[\frac{\varkappa_T}{\varkappa_\parallel}\frac{\partial^2 Q}{\partial \tilde{z}^2} - 8\frac{\partial}{\partial \tilde{z}}\left(\sqrt{Q} - Q\right)\right] - \frac{\partial Q}{\partial \tilde{z}} = 0, \quad (13)$$

where the coefficients $\tilde{K}_\perp = \left(1 + \frac{v_0}{6c(1-\sqrt{Q})}\left|\frac{\partial Q}{\partial \tilde{r}}\right|\right)^{-1}$ and $\tilde{K}_\parallel = \left(1 + \frac{\varkappa_T}{\varkappa_\parallel}\frac{v_0}{6c(1-\sqrt{Q})}\left|\frac{\partial Q}{\partial \tilde{z}}\right|\right)^{-1}$ are calculated at each consecutive iteration using values of $Q$ obtained in the previous iteration.

Equation (13) was solved numerically using the finite difference approximation method. A time-relaxation scheme was used. In this approach, the equation in the form $L[Q] = 0$, where $L$ is the corresponding differential operator, has been replaced by a parabolic equation of the form $\frac{\partial Q}{\partial t} - L[Q] = 0$. The steady-state solution of the last equation coincides with the solution of the original elliptic equation. An explicit finite-difference scheme was used to solve the parabolic equation.

### 3.3 Results of numerical calculations

Numerical simulations were carried out for accretion rates onto one pole in the range $10^{17} - 1.2 \times 10^{18}$ g s$^{-1}$ for the hollow cylinder geometry and the filled cylinder geometry. The column structure at different accretion rates is shown in Fig. 2. Note that at a given mass accretion rates and the NS magnetic field, the height of the braking zone in the hollow cylinder case is smaller than that in the case of the filled cylinder, as expected from the dependence of the radiation diffusion time on the wall thickness $\propto b$. Clearly, in very geometrically thin walls, $b/r_0 \ll 1$, the flow will be optically thin as well (at least for the extraordinary mode with angle-independent scattering cross-section in the strong magnetic field). This may suggest that even if the flow was initially confined within a thin layer, near the NS surface the huge energy release may change the character of the flow. This possibility is worth investigating further.

Guided by the velocity braking in a radiation-dominated shock, $v \approx 1/7 v_0$, we define the 'height' of the accretion mound $z_0(\dot{M})$ as the distance at the centre of the structure where the gas flow velocity is reduced to one seventh of the initial value. The (dimensionless) height calculated for different accretion rates were fitted by a power law

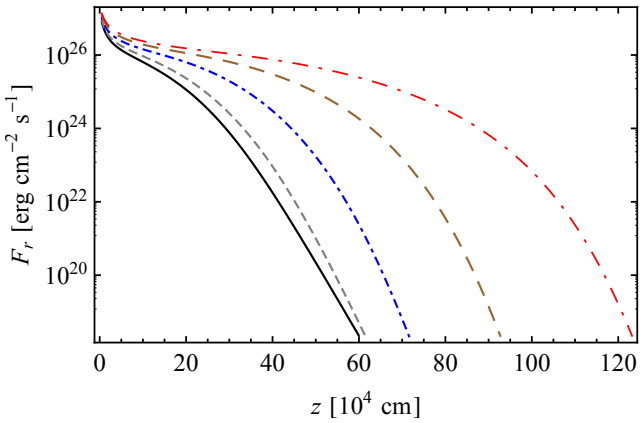


**Figure 3.** The radial energy flux $F_r(\tau = 2/3, z)$ calculated along the height of a filled cylinder column at different mass accretion rates. Half of this flux (extraordinary photons only) escapes sidewall. The lines from bottom to up correspond to $\dot{M}_{17} = 2$, 3, 5, 8 and 12, respectively.

$$\tilde{z}_0 = \beta \dot{M}_{17}^\alpha, \quad (14)$$

where $\tilde{z}_0 = \varkappa_T S_0 z_0/c$. We found that in both geometries $\alpha \sim 1$ and $\beta > 0$ ($\alpha \simeq 1.1, \beta \simeq 0.3$ for the case of hollow cylinder and $\alpha \simeq 0.9$, $\beta \simeq 13.5$ for the filled cylinder). Therefore, the numerical solution behaves in agreement with the qualitative physical considerations about the structure of optically thick accretion mounds described above.

## 4 CHANGE IN THE HARDNESS RATIO FROM ACCRETION COLUMNS

### 4.1 Saturated Compton spectrum of sidewall emission

The LTE treatment of the spectrum of the sidewall emission from accretion columns is clearly a strong oversimplification. To take into account the scattering on electrons in the optically thin boundary of the column, we can use the model calculations of the radiation transfer problem in a semi-infinite plane-parallel atmosphere with strong magnetic field. In this case the emerging spectrum will be formed in the saturated Compton regime, with the mode 1 photons (extraordinary, i.e. polarized perpendicular to the $\boldsymbol{k} - \boldsymbol{B}$-plane, where $\boldsymbol{k}$ is the photon wavevector and $\boldsymbol{B}$ is the magnetic field vector) predominantly escaping through sidewalls (Lyubarskii 1986). The intensity of mode 2 (ordinary, i.e. polarized in the $\boldsymbol{k} - \boldsymbol{B}$ plane) photons is comparable to that of mode 1 photons only at large angles to the normal, $\mu' \sim 0$, and thus insignificantly contribute to the total flux from the unit surface area due to the geometrical factor.

In this regime, the specific intensity of extraordinary photons at energies far below the cyclotron resonance can be written to an accuracy of a few per cents as (Lyubarskii 1986)

$$I'_\nu = \frac{2\sqrt{3}}{5}(1 + 2\mu')\frac{h\nu\nu_g^2}{c^2\tau_0}e^{-\frac{h\nu}{kT}}, \quad (15)$$

where $\mu' = \cos\theta'$ is the angle between the normal to the atmosphere and the escaping radiation direction in the plasma reference frame, $\tau_0$ is the characteristic optical depth of the problem, $\nu_g = \frac{eB}{2\pi m_e c}$ is the electron gyrofrequency in the magnetic field. By expressing the characteristic optical depth $\tau_0$ through the emergent radiation flux $\Phi$ using Eqs. (34-37) from Lyubarskii (1986), we find

$$I'_\nu = \frac{3}{10\pi}\left(\frac{h\nu}{kT}\right)^2 \frac{\Phi}{\nu}e^{-\frac{h\nu}{kT}}. \quad (16)$$

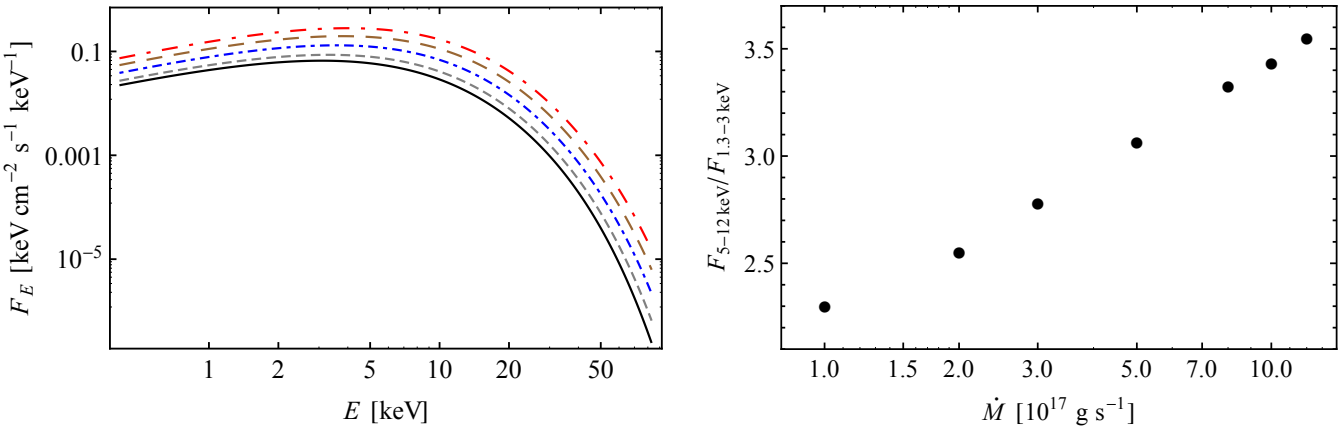


**Figure 4.** Left: The spectrum of sidewall emission from optically thick filled cylinder accretion column (16) for mass accretion rates $\dot{M}_{17} = 2$, 3, 5, 8 and 12 (from bottom to up, respectively). Right: The spectral hardness ratio $HR$ as a function of mass accretion rate.

Therefore, we are in the position to calculate the emerging spectrum from the column in this approximation using the solutions for the column structure obtained above. To do this, it is sufficient to substitute the total radial energy flux at each height of the column $\Phi \to F_r(z)/2$, and temperature $T \to T(z)$ estimated deep inside the column (at the optical depth $\sim 1$), so that $T(z) = (U(z)/a_r)^{1/4}$). Note here that at large optical depth the number density of ordinary and extraordinary photons are equal, with the extraordinary photons becoming overwhelmingly dominant in the optically thin outer layers. Therefore, only half of the radial energy flux, $F_r(z)/2$, should be taken into account in the spectral calculations. The second half of the radial flux (in ordinary photons) is admixed to the vertical energy flux component, $F_z$. Some fraction of this energy flux can propagate (mostly as ordinary photons) along the magnetic field into the optically thin upper part of the column; we do not calculate their fate in this paper and restrict ourselves by this quantitative note. The radial energy flux $F_r(z)$ from the filled column is shown in Fig. 3 for different mass accretion rates.

The resulting spectra of the sidewall emission from the optically thick accretion column integrated over the column height $z$ is shown in Fig. 4 (left panel) for the case of the filled column and different $\dot{M}$. The spectral hardness ratio

$$HR = \frac{\int\limits_{5\ \mathrm{keV}}^{12\ \mathrm{keV}} F_\nu d\nu}{\int\limits_{1.3\ \mathrm{keV}}^{3\ \mathrm{keV}} F_\nu d\nu}, \qquad (17)$$

is shown in the right panel of this figure as a function of $\dot{M}$. It is seen that the hardness ratio of the spectrum of the column monotonically increases with mass accretion rate.

### 4.2 Account for the reflected component

We have seen that the saturated-Comptonized spectrum of sidewall emission from optically thick accretion column gets harder with increasing $\dot{M}$, contrary to what is observed and discussed above. However, an important feature of accretion in X-ray pulsars should be added at this point. Namely, we should take into account the fact that the electrons in the optically thin part of the column are moving with high velocity $v_0 \sim 1/3c$, and thus the emission beam

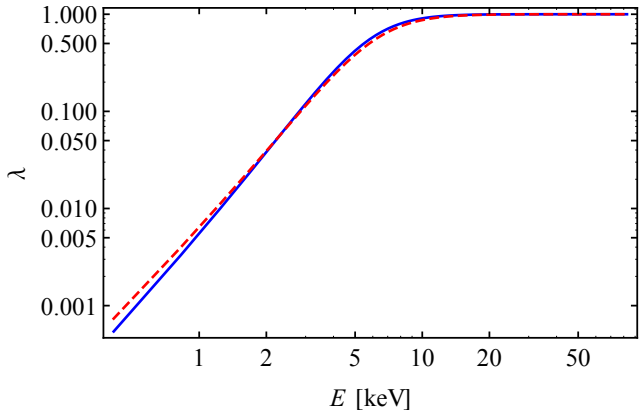


**Figure 5.** The single-scattering Compton X-ray albedo from a plane-parallel neutron star atmosphere with strong magnetic field. The electron number density is $n_e = 5 \times 10^{25}$ cm$^{-3}$, electron temperature $T = 3$ keV, magnetic field $B = 3 \times 10^{12}$ G, photon incident angle to the magnetic field $\pi/4$. Extraordinary and ordinary photon spectra are shown by the solid and dashed lines, respectively. The cyclotron line is ignored.

of the column (15) should be Doppler-boosted towards the neutron star surface and reflected from the neutron star atmosphere, as discussed in Lyubarskii & Syunyaev (1988) and Poutanen et al. (2013). The reflection coefficient in the case of single Compton electron scattering in strong magnetic field is determined by the ratio $\lambda(\nu) = \kappa_{sc}/(\kappa_{sc} + \kappa_{abs})$, where $\kappa_{sc}$ and $\kappa_{abs}$ is the scattering and absorption coefficients for photons in the strong magnetic field, respectively. The reflection coefficient (X-ray albedo) is calculated in the Appendix A and is presented in Fig. 5. Note that the calculated X-ray albedo turns out to be very similar for both extraordinary and ordinary photons and is virtually insensitive to the photon incident angle to the magnetic field. Everywhere below we shall use X-ray albedo for extraordinary photons only. It is seen that soft photons are mostly absorbed, while hard photons are reflected by the neutron star atmosphere. Therefore, the reflected spectrum is harder than the incident one.

Let $\alpha$ be the angle between the photon wavevector and the plasma bulk velocity vector. Due to the boosting, part of radiation from the column will be intercepted by the neutron star surface and

reflected. The critical angle $\alpha^*$ within which the radiation from the height $z$ above the surface will be intercepted by the neutron star (in the Schwarzschild metric) is (Poutanen et al. 2013)

$$\sin\alpha^* = \frac{R_{NS}}{R_{NS}+z}\sqrt{\frac{1-r_S/(R_{NS}+z)}{1-r_S/R_{NS}}}, \quad (18)$$

where $r_S = 2GM/c^2$ is the Schwarzschild radius. The difference between the polar axis and the column cylinder side can be neglected for $r_0 \ll R_{NS}$.

Let $\Sigma$ be the surface of the column, $\Sigma'(\varphi, z)$ be a point on the surface and $d\Sigma = r_0 d\varphi dz$ be the elementary area. The flux from the surface element at frequency $\nu$ (in conventional notations) reads

$$f_\nu(\Sigma') = \frac{dE(\Sigma')}{dtd\nu r_0 d\varphi dz} \quad (19)$$

and can be separated into three parts in accordance to the angle relative to the observer. Photons escaping with angles $\alpha > \alpha^*$ to the column are directly seen as the proper column radiation $f_\nu^{col}$. The second part includes the radiation $f_\nu^{ref}$ intercepted by the neutron star and reflected from the neutron star surface with X-ray albedo $\lambda(\nu)$. The third part $f_\nu^{abs}$ is the radiation absorbed and re-radiated by the neutron star atmosphere. Then we can write:

$$\begin{aligned} f_\nu(\Sigma') &= \int_{-1}^{1} \frac{df_\nu(\Sigma')}{d\cos\alpha} d\cos\alpha \\ &= \int_{-1}^{\cos\alpha^*} \frac{df_\nu(\Sigma')}{d\cos\alpha} d\cos\alpha + \int_{\cos\alpha^*}^{1} \frac{df_\nu(\Sigma')}{d\cos\alpha} d\cos\alpha \\ &= \int_{-1}^{\cos\alpha^*} \frac{df_\nu(\Sigma')}{d\cos\alpha} d\cos\alpha \\ &+\lambda(\nu)\int_{\cos\alpha^*}^{1} \frac{df_\nu(\Sigma')}{d\cos\alpha} d\cos\alpha + (1-\lambda(\nu))\int_{\cos\alpha^*}^{1} \frac{df_\nu(\Sigma')}{d\cos\alpha} d\cos\alpha \\ &= f_\nu^{col}(\Sigma') + f_\nu^{ref}(\Sigma') + f_\nu^{abs}(\Sigma'). \end{aligned} \quad (20)$$

The integrands (Poutanen et al. 2013) in the cylindrical coordinates with account for the axial symmetry ($I_\nu(\Sigma') = I_\nu(z)$, giving by (15)) have the form:

$$\frac{df_\nu(\Sigma')}{d\cos\alpha} = I_\nu(z)\frac{2D^3}{\gamma}\sin\alpha\left(1+\frac{\pi D}{2}\sin\alpha\right), \quad (21)$$

where the Doppler factor is $D = 1/(\gamma(1-\beta\cos\alpha))$, $\gamma = 1/\sqrt{1-\beta^2}$ is the plasma Lorentz factor and $\beta = v/c$. Here we have taken into account that the specific flux (per unit frequency interval) is $D$ times as small as the integral flux. Then for the total radiation from the column at frequency $\nu$ we obtain:

$$\begin{aligned} L_\nu &= \iint_\Sigma f_\nu(\Sigma')d\Sigma = 2\pi r_0 \int_0^{z_{max}} f_\nu(z)dz \\ &= 2\pi r_0 \int_0^{z_{max}} (f_\nu^{col}(z) + f_\nu^{ref}(z) + f_\nu^{abs}(z))dz \\ &= L_\nu^{col} + L_\nu^{ref} + L_\nu^{abs}, \end{aligned} \quad (22)$$

where $z_{max}$ is the upper limit of the computational area. The observed X-ray flux from one column is $F_\nu = (L_\nu^{col} + L_\nu^{ref})/(4\pi d^2)$, where $d$ is the distance to the source. For the illustrative purposes, we assume $d = 5$ kpc. Taking into account of the radiation absorbed by the neutron star atmosphere $L_\nu^{abs}$ will add more soft photons to the total spectrum.

Since we are observing both the direct and reflected radiation from the column, the total change in the hardness of the spectrum will depend on the fraction of the reflected radiation in the total flux. This, in turn, depends on the height of the column. We have calculated the total flux as the sum of the direct and reflected component as a function of $\dot{M}$ with taking into account the photon ray propagation in the Schwarzschild metric of the neutron star with a fiducial mass $M = 1.5M_\odot$ and radius $R = 10$ and 13 km. The magnetic field of the neutron star is set to $3\times10^{12}$ G, so that the CRSF energy is about 35 keV. The result is presented in Fig. 6. It is seen that the hardness ratio $HR$ first increases with the mass accretion rate (X-ray luminosity), but starting from $\dot{M}_{cr} \sim (6-8)\times10^{17}$ g s$^{-1}$ it gets saturated and even decreases. This is in agreement with observations shown in Fig. 1.

For the hollow cylinder accretion columns which have smaller height (see Fig. 2), the fraction of the reflected component in the total emission does not virtually change with mass accretion rate within the calculated range, therefore the hardness ratio of the total spectrum monotonically increases with $\dot{M}$ in this range (see Fig. 7). Note also that in this case the spectrum is harder than in the case of the filled column because the reflected (harder) emission dominates in the total spectrum.

## 5 SUMMARY AND CONCLUSIONS

In this paper, using RXTE/ASM archival data we studied the behaviour of the spectral hardness ratio as a function of X-ray luminosity at different accretion rates in a sample of six transient X-ray pulsars (EXO 2030+375, GX 304-1, 4U 0115+63, V 0332+63, A 0535+26 and MXB 0656-072). In all cases, the hardness ratio is found to increase with X-ray flux at low luminosities and then to saturate or even slightly to decrease above some critical luminosity of a few times $10^{37}$ erg s$^{-1}$ This behaviour confirms earlier findings by Reig & Nespoli (2013), and Klochkov et al. (2011) and correlates with the behaviour of the CRSF energy with flux in the CRSF sources.

At low mass accretion rates and low X-ray luminosities, the braking of infalling matter is expected to be mediated by Coulomb interactions (Zel'dovich & Shakura 1969; Nelson, Salpeter & Wasserman 1993; Becker et al. 2012) and occurs close to the neutron star surface, essentially at a height of the homogeneous atmosphere above the neutron star surface, without the formation of an accretion column. When the X-ray luminosity increases above some critical value $\sim 10^{37}$ erg s$^{-1}$ (Davidson 1973; Basko & Sunyaev 1976; Wang & Frank 1981; Mushtukov et al. 2015), the radiation pressure of generated photons decelerates the infalling matter. An optically thick accretion column arises with the height increasing almost linearly with accretion rate.

Therefore, at low luminosities $< L^* \sim 10^{37}$ erg s$^{-1}$ the emerging X-ray spectrum is essentially formed by ordinary photons in a magnetized optically thin atmosphere. The hardness of the spectrum is determined by the Comptonization $y$-parameter, $y = (kT/m_ec^2)\tau$, which increases with accretion rate. This implies that in this case the hardness of the emerging radiation will increase with luminosity.

At higher luminosities an optically thick accretion column above the magnetic pole arises, and thermal radiation generated deep inside the column escapes sidewall predominantly as extraordinary photons. Since at energies far less than the CRSF energy the electron scattering cross-section strongly decreases with frequency, the spectrum of the emergent continuum radiation will be softer than the diluted Wien spectrum expected to be formed in the saturated Compton regime, $\sim \nu e^{-h\nu/kT}$ Lyubarskii (1986).

We have calculated the structure of axially symmetric opti-

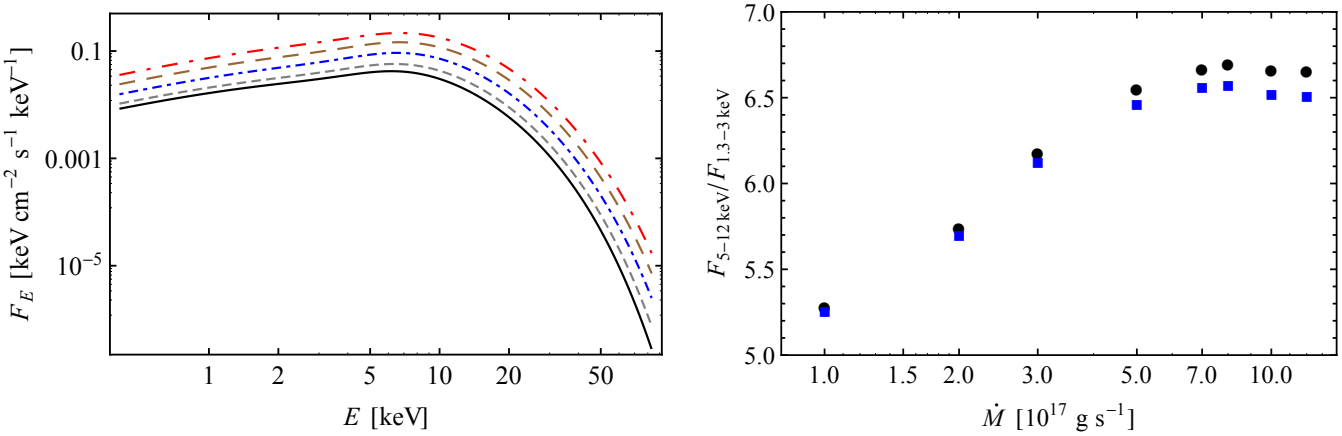


**Figure 6.** Left: the total spectrum of direct sidewall and reflected from the neutron star atmosphere from the optically thick filled accretion column for mass accretion rates $\dot{M}_{17} = 2$, 3, 5, 8 and 12 (from bottom to up, respectively). Right: the hardness ratio $HR$ of the total spectrum. Shown are calculations for the neutron star radius $R_{NS} = 10$ km (squares) and $R_{NS} = 13$ km (circles).

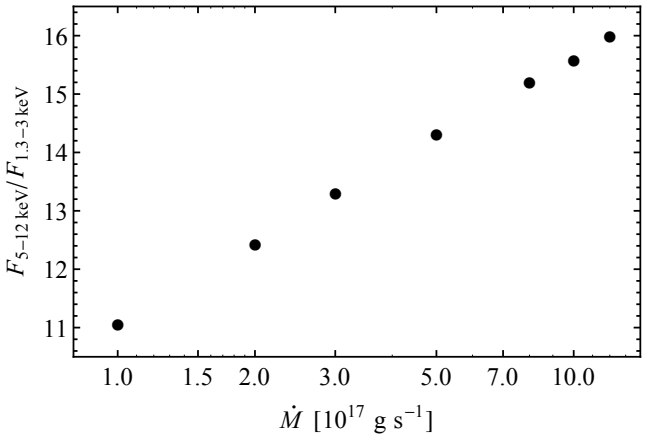


**Figure 7.** Hardness ratio of the total emission (direct plus reflected from the neutron star atmosphere) from a hollow cylinder accretion column with $b = 0.1r_0$ as a function of mass accretion rate $\dot{M}$.

cally thick accretion columns in the diffusion approximation for radiation transfer for different mass accretion rates. Two accretion column geometries, filled cylinder and hollow cylinder, were considered. In both cases we have found the expected almost linear growth of the column height with mass accretion rate. The continuum X-ray spectrum of the sidewall emission in both geometries gets harder with increasing mass accretion rate. Taking into account of the radiation reflected from the neutron star atmosphere allowed us to reproduce the observed saturation of the continuum hardness. This is purely geometrical effect: with increasing mass accretion rate the height of the column increases, so does the fraction of the reflected radiation. However, starting from some height, the fraction of the reflected radiation in the total flux stops increasing and starts decreasing. Since the hardness of the reflected radiation is higher than that of the incident emission (because of the strong energy dependence of the scattering and absorption coefficients in the strong magnetic fields), the hardness of the total spectrum (direct sidewall emission from the accretion column plus reflected radiation from the neutron star atmosphere) saturates (and even can slightly decrease) beyond some characteristic mass accretion rate $\sim (6-8)\times 10^{17}$ erg s$^{-1}$ for the typical neutron star parameters: $M_{NS} = 1.5M_\odot$, $R_{NS} = 10$ km and 13 km, $B = 3\times 10^{12}$ G.

In the case of the hollow cylinder accretion column geometry with a fiducial wall thickness of 0.1 the outer column radius $r_0$, we have not found the spectral hardness ratio saturation with increasing mass accretion rate up to the maximum value of our calculations $1.2\times 10^{18}$ g s$^{-1}$. Apparently, the height of the column in this case is too low, the hard reflected component dominates at all mass accretion rates, and the (softer) direct sidewall emission remains subdominant in the total spectrum.

Therefore, our model calculations lead to the following conclusions.

1. The spectral hardening in X-ray pulsars with positive CRSF energy dependence on X-ray flux can be explained by increasing of the Comptonization parameter $y$ in the slab atmosphere of the accretion mound. It is in this regime that positive correlation of the cyclotron line is observed, for example, in Her X-1 (Staubert et al. 2007).

2. At high accretion rates, the radiation-supported optically thick accretion column grows above the polar cap, the sidewall emission from the column is formed by extraordinary photons in the saturated Compton regime. The spectrum of this emission gets harder with increasing mass accretion rate.

3. With further increasing mass accretion rate the height of the column increases, such that the fraction of radiation reflected from the neutron star atmosphere starts decreasing. As the reflected radiation is harder than the incident one, the spectrum of the total emission (direct plus reflected) stops hardening (and even becomes slightly softer). This happens at the mass accretion rate onto one pole $\dot{M}_{cr} \sim (6-8)\times 10^{17}$ g s$^{-1}$, in qualitative agreement with observations (see Fig. 1).

4. In the frame of this model, the saturation of the spectral hardness in the case of a hollow cylinder geometry of the accretion column can be achieved at much higher accretion rates (roughly, scaled with the relative thickness of the column wall, $r_0/b$), because the characteristic height of the column in this case is correspondingly smaller than that of the filled column.

5. Variations in the pulse profile form and polarization properties during the transition from the Coulomb-braking low-luminosity regime to the radiation-braking high-luminosity state should occur with changing mass accretion rate (X-ray luminosity)

in accreting X-ray pulsars. The profile change has already been reported during the low-states in Vela X-1 (Doroshenko, Santangelo & Suleimanov 2011).

We conclude that X-ray continuum observations in transient X-ray pulsars can be used as additional diagnostic of different accretion regimes and column geometry near the surface of highly magnetized neutron stars.

## 6 ACKNOWLEDGEMENTS

MG, NSh, VL and acknowledge the Russian Science Foundation grant 14-12-00146. The work of KP and DK is supported by RFBR/DFG grant KL 2734/2-1 (RFBR-NNIO 14-02-91345).

## REFERENCES

Arons J., 1992, ApJ, 388, 561
Basko M. M., Sunyaev R. A., 1975, A&A, 42, 311
Basko M. M., Sunyaev R. A., 1976, MNRAS, 175, 395
Becker P. A. et al., 2012, A&A, 544, A123
Boldin P. A., Tsygankov S. S., Lutovinov A. A., 2013, Astronomy Letters, 39, 375
Caballero I., Wilms J., 2012, Mem. Soc. Ast. It., 83, 230
Davidson K., 1973, Nature Physical Science, 246, 1
Doroshenko V., Santangelo A., Suleimanov V., 2011, A&A, 529, A52
Fürst F. et al., 2014, ApJ, 780, 133
Giacconi R., Gursky H., Kellogg E., Schreier E., Tananbaum H., 1971, ApJL, 167, L67
Ho W. C. G., Lai D., 2001, MNRAS, 327, 1081
Klein R. I., Arons J., Jernigan G., Hsu J. J.-L., 1996, ApJL, 457, L85
Klochkov D. et al., 2012, A&A, 542, L28
Klochkov D., Staubert R., Santangelo A., Rothschild R. E., Ferrigno C., 2011, A&A, 532, A126
Kühnel M. et al., 2014, in European Physical Journal Web of Conferences, Vol. 64, European Physical Journal Web of Conferences, p. 6003
Lutovinov A. A., Tsygankov S. S., Suleimanov V. F., Mushtukov A. A., Doroshenko V., Nagirner D. I., Poutanen J., 2015, MNRAS, 448, 2175
Lyubarskii Y. É., 1986, Astrophysics, 25, 577
Lyubarskii Y. E., Syunyaev R. A., 1988, Soviet Astronomy Letters, 14, 390
McBride V. A. et al., 2006, A&A, 451, 267
Mihara T., Makishima K., Nagase F., 2004, ApJ, 610, 390
Müller S. et al., 2013, A&A, 551, A6
Mushtukov A. A., Suleimanov V. F., Tsygankov S. S., Poutanen J., 2015, MNRAS, 447, 1847
Nagel W., 1980, ApJ, 236, 904
Negueruela I., Okazaki A. T., 2001, A&A, 369, 108
Negueruela I., Roche P., Fabregat J., Coe M. J., 1999, MNRAS, 307, 695
Nelson R. W., Salpeter E. E., Wasserman I., 1993, ApJ, 418, 874
Nishimura O., 2014, ApJ, 781, 30
Parkes G. E., Murdin P. G., Mason K. O., 1980, MNRAS, 190, 537
Poutanen J., Mushtukov A. A., Suleimanov V. F., Tsygankov S. S., Nagirner D. I., Doroshenko V., Lutovinov A. A., 2013, ApJ, 777, 115
Reig P., Nespoli E., 2013, A&A, 551, A1
Revnivtsev M., Mereghetti S., 2014, Space Sci. Rev.
Staubert R., Shakura N. I., Postnov K., Wilms J., Rothschild R. E., Coburn W., Rodina L., Klochkov D., 2007, A&A, 465, L25
Steele I. A., Negueruela I., Coe M. J., Roche P., 1998, MNRAS, 297, L5
Tsygankov S. S., Lutovinov A. A., Churazov E. M., Sunyaev R. A., 2006, MNRAS, 371, 19
Tsygankov S. S., Lutovinov A. A., Churazov E. M., Sunyaev R. A., 2007, Astronomy Letters, 33, 368
Tsygankov S. S., Lutovinov A. A., Serber A. V., 2010, MNRAS, 401, 1628
Ventura J., 1979, Phys. Rev. D, 19, 1684
Virtamo J., Jauho P., 1975, Nuovo Cimento B Serie, 26, 537
Wang Y.-M., Frank J., 1981, A&A, 93, 255
Wilson C. A., Finger M. H., Coe M. J., Laycock S., Fabregat J., 2002, ApJ, 570, 287
Yamamoto T., Sugizaki M., Mihara T., Nakajima M., Yamaoka K., Matsuoka M., Morii M., Makishima K., 2011, PASJ, 63, 751
Zel'dovich Y. B., Shakura N. I., 1969, Sov. Astron., 13, 175

## APPENDIX A: X-RAY ALBEDO FROM NEUTRON STAR ATMOSPHERE

The X-ray albedo (the fraction of the reflected to incident flux) from the neutron star atmosphere in strong magnetic field in the general case depends on the angle between the incident photon and the magnetic field and the photon polarization. Not solving exactly the problem, we calculate single-scattering albedo for a plane-parallel atmosphere $\lambda^j(\nu)$ ($j = 1, 2$ for extraordinary and ordinary photon polarizations, respectively):

$$\lambda^j(\nu) = \frac{\kappa^j_{sc}}{\kappa^j_{sc} + \kappa^j_{abs}}, \tag{A1}$$

where $\kappa^j_{sc}$ and $\kappa^j_{abs}$ are scattering and absorption coefficients in the magnetic field, respectively.

We calculate the coefficients following Ventura (1979); Nagel (1980); Ho & Lai (2001). The electron and ion scattering coefficients for mode $j$ reads:

$$\kappa^j_{sc,e} = n_e \sigma_T \sum_{\alpha=-1}^{1} \frac{\omega^2}{(\omega + \alpha\omega_{c,e})^2} |e^j_\alpha|^2 \tag{A2}$$

$$\kappa^j_{sc,i} = \left(\frac{Z^2 m_e}{A m_p}\right)^2 n_i \sigma_T \sum_{\alpha=-1}^{1} \frac{\omega^2}{(\omega + \alpha\omega_{c,i})^2} |e^j_\alpha|^2 \tag{A3}$$

where $\sigma_T$ is the Thomson scattering cross-section, $m_e$ and $m_p$ is the electron and proton masses, $n_e$ and $n_i$ is electron and ion concentrations, $\omega_{c,e}$ and $\omega_{c,i}$ is the electron and ion cyclotron angular frequency, $e^j_{-1}$, $e^j_1$, are $e^j_0$ are the components of the photon polarization vector $\mathbf{e}^j$ for mode $j$ (see subsection 2.5 and Appendix A in (Ho & Lai 2001)). The absorption coefficients are

$$\kappa^j_{abs,e} = \kappa_0 \sum_{\alpha=-1}^{1} \frac{\omega^2}{(\omega + \alpha\omega_{c,e})^2} |e^j_\alpha|^2 g_\alpha \tag{A4}$$

$$\kappa^j_{abs,i} = \left(\frac{Z^2 m_e}{A m_p}\right)^2 \frac{\kappa_0}{Z^3} \sum_{\alpha=-1}^{1} \frac{\omega^2}{(\omega + \alpha\omega_{c,i})^2} |e^j_\alpha|^2 g_\alpha \tag{A5}$$

where

$$\kappa_0 = 4\pi^2 Z^2 \alpha^3 \left(\frac{\hbar c}{m_e}\right)^2 \left(\frac{2m_e}{\pi kT}\right)^{1/2} \frac{n_e n_i}{\omega^3} \left(1 - e^{-\frac{\hbar\omega}{kT}}\right) \tag{A6}$$

is the free-free absorption coefficient in the absence of a magnetic field, $g_{\pm1}$ and $g_0$ are the modified Gaunt-factors (Nagel 1980),

$$g_{\pm1} = \int_{-\infty}^{\infty} \exp\left(-\frac{\hbar\omega}{kT} \sinh^2 x\right) C_1\left(\frac{\omega}{\omega_c} e^{2x}\right) dx, \tag{A7}$$

$$g_0 = \int_{-\infty}^{\infty} \exp\left(-\frac{\hbar\omega}{kT} \sinh^2 x\right) 2\frac{\omega}{\omega_c} e^{2x} C_0\left(\frac{\omega}{\omega_c} e^{2x}\right) dx. \tag{A8}$$

Here $\omega_c$ is electron (ion) cyclotron angular frequency. Functions $C_1$ and $C_0$ are calculated in Virtamo & Jauho (1975). The total coefficients are:

$$\kappa^j_{sc} = \kappa^j_{sc,e} + \kappa^j_{sc,i}, \tag{A9}$$

$$\kappa^j_{abs} = \kappa^j_{abs,e} + \kappa^j_{abs,i}. \tag{A10}$$

The coefficients $\kappa_{sc}$ and $\kappa_{abs}$ depend on many factors. They are determined by the characteristic of reflecting atmosphere, including the chemical composition, ion number density and temperature, as well as by the photon incident angle to the magnetic field and the magnetic field strength. The last two parameters turn out to be weakly changing the X-ray albedo $\lambda^j(\nu)$ in the interesting range of parameters (see Fig. 5). In the calculations we have assumed purely hydrogen atmosphere with ion charge $Z = 1$, the mass number $A = 1$ and the ion number density $n_i = 5 \times 10^{25}$ cm$^{-3}$ (it can be higher in deeper layers (Ho & Lai 2001)). The electron temperature is fixed at $T = 3$ keV, which corresponds to the expected Compton temperature during reflection of X-ray emission form the column.

The single-scattering X-ray albedo as a function of frequency for ordinary ($j = 2$) and extraordinary ($j = 1$) photon polarizations is shown in Fig. 5.